IEEE Access
Multidisciplinary : Rapid Review : Open Access Journal

Received October 11, 2020, accepted October 17, 2020, date of publication October 20, 2020, date of current version October 30, 2020.

Digital Object Identifier 10.1109/ACCESS.2020.3032563

Design of LCC-S Compensation Topology and Optimization of Misalignment Tolerance for Inductive Power Transfer

JUNFENG YANG[1], (Member, IEEE), XIAODONG ZHANG[1,3], KAIJIAN ZHANG[2], XIAOYAN CUI[4], CHAOQUN JIAO[1], AND XU YANG[1], (Student Member, IEEE)

[1]School of Electrical Engineering, Beijing Jiaotong University, Beijing 100044, China
[2]School of Computer Science and Engineering, University of New South Wales, Sydney, NSW 2052, Australia
[3]Beijing Jiaotong University Haibin College, Huanghua 061199, China
[4]School of Automation, Beijing University of Posts and Telecommunications, Beijing 100876, China

Corresponding author: Xiaodong Zhang (xdzhang@bjtu.edu.cn)

This work was supported in part by the Fundamental Research Funds for the Central Universities under Grant 2019YJS168.

ABSTRACT This paper proposes a novel parameter tuning method topology for inductive power transfer (IPT) system with excellent load-independent current output. Based on LCC-S compensation topology, detailed derivations of parameters to realize load-independent current output is systematically analyzed. The realizations of zero voltage switching (ZVS) and reactive power demand are discussed by theoretical deduction and numerical simulation. Moreover, from the perspective of maintaining stable transmission power, the parameters detuning method to enhance misalignment tolerance is presented. Theoretical analysis shows that the appropriate detuned resonant tank is advantageous in performance, especially the smoothing of current output to variation of coupling coefficient. The novel LCC-S compensation topology holds high design freedom and high efficiency, while the robust power characteristic against wide misalignment region minimizes the need of complex control. Finally, the IPT prototype is built and test to validate the feasibility of the proposed topology. The efficiency of system is always higher than 86% in tuned parameters and 73% in detuned condition. The fluctuation of current is less than 7.5% when the coupling coefficient varies almost 170% (from 0.293 to 0.5).

INDEX TERMS Inductive power transfer (IPT), compensation network, zero voltage switching (ZVS), misalignment tolerance.

I. INTRODUCTION

Inductive power transfer (IPT) systems with advantages of convenience of use, isolation, safe operation and environment friendly have attracted considerable attention in last several years [1], [2]. High efficiency and steady power transfer is the first and uppermost objectives for all IPT power applications. For some scenarios such as moving EVs, a certain degree of mobility freedom is further required [3], [4]. In view of these problems, many researches have been carried out, including compensation topology optimization and circuit analyses [5]–[7], magnetic couplers design [8]–[10], control algorithm for obtaining desired characteristics [11]. Among these methods, compensation topology and circuit analyses are vital for its determination of resonant frequency, output characteristics, power factor [12].

It is well known that the leakage inductors of loosely coupled transformer (LCT) is needed to be compensated in an IPT system to transfer real power to the load side. Several compensation networks have been put forward to compensate primary side and/or secondary side. Their goals are mainly to achieve or improve the following desirable characteristics [7], [13]: A constant current/constant voltage output, independent of load resistance; A weak inductive input impedance to achieve zero voltage switching (ZVS), which can realize high efficiency through soft switching; Less sensitivity to the variable coupling coefficient, which can greatly expand the scope of applications. In general, it is difficult for a compensation circuit to fulfill all the above characteristics in an IPT system. Initially, four basic compensation topologies,

The associate editor coordinating the review of this manuscript and approving it for publication was Kai Song.

namely, serial-serial (SS), serial-parallel (SP), parallel-serial (PS), and parallel-parallel (PP), are widely used in many scenarios. Among these four topologies, SS compensation topology possesses more desirable characteristics: achieving zero voltage switching and near zero reactive power, without suffering from bifurcation phenomena [14]. Only two compensation capacitors are necessary for SS topology, resulting in less power loss, smaller size, higher power density and lower cost. However, once the transformer is determined, the transfer performance of converter is almost fixed unless a new LTC is replaced. Moreover, when relative position of two coils changes, the performance of IPT system deteriorates rapidly. When the coupling coefficient of the employed LCT decreases to zero, the equivalent load for the voltage source is also close to zero. Infinite currents through primary capacitor and inductor are created, resulting in an additional protection circuit in such system [15]. Low design freedom and high sensitivity to misalignment highly restrict the practical promotion of SS-compensated IPT system.

In order to solve the problem of ultra-large current in SS topology, higher order compensation methods, such as LCL compensation topology is proposed [16]. The added compensation inductance balance the power transaction between inverter and resonant tank. The primary coil current behaves like a current source, providing stable voltage for the secondary side through magnetic coupling. Hou *et al.* [17] developed an alternative model to realize soft switching and decrease reactive power. The determined compensation inductance is selected to equal to the self-inductance of coils, which is quite large and deficient of low design freedom. This deficiency was solved in [18]–[21] by introducing another capacitor in series with coupling coils, which usually named LCC topology. Many works [20], [22], [23] have adopted this strategy and demonstrate higher and stable efficiency. The LCC compensation topologies provide many desirable performances, such as ZPA operations, high freedom of design, but more resonant elements, resulting in complex tune and the increase of system size and cost.

Another focus of researches is to improve misalignment tolerance. The relative position between the primary and secondary coils is normally changeable, introducing variations in inductances and coupling coefficient of the LCT. In [24], with complicated parameter optimization, LCC compensation topology presents more robust voltage output characteristic: the power drop is less than 20% against 200% variation of coupling coefficient (from 0.16 to 0.32 or from 0.15 to 0.3). However, three compensation elements in the primary side need to be optimized, where the compensation inductance and series capacitance are designed to satisfy ZVS, and parallel capacitance is employed to meet the output power demand. Dependent on the designed coupling coefficient, a high misalignment tolerant S/SP type compensation topology is lucubrated [25]. The robust reaction to both coupling coefficient and load variation are analyzed. In [26], full-bridge dual resonant tank topology is proposed to improve efficiency when lateral misalignment occurs in an IPT system. It is necessary to balance the voltage on the two support capacitors. The composite circuits and additional components lessen the system controllability. A μ-controller designed in [27] is used to set up a closed-loop system for SP topology. Robust stability and performance are obtained for coils misalignment in 3-D directions. In practice, a great deal of loads, such as batteries need stable current charging profile against coupling coefficient. A detuning optimization method is applied in SS topologies [28], composing the primary inductively and secondary capacitively tuned (PISC) system. The modified method needs two-sided adjustment and does not take into account variable load. Therefore, a novel LCC-S compensation topology with the characteristic of excellent constant current output is provided in this paper. It has the advantages of high design freedom, easy ZVS achievement and no control circuit required. By optimizing of two primary side detuning parameters, the transmit power against varied load and misalignment simultaneously can be maintained.

This paper is structured as follows. The excellent load-constant current output (CCO) characteristic and the realization of ZVS are analyzed in Section II firstly. Considering robustness and steady performance, the method to enhance misalignment tolerance is proposed in Section III. A 100-W practical IPT prototype is designed and manufactured in Section IV. Finally, Section V concludes this paper.

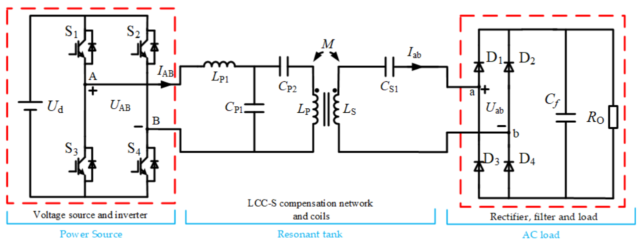

FIGURE 1. Circuit diagram of LCC-S compensated IPT system.

II. TOPOLOGY DESIGN

Composed of three parts, power supply, resonant tank and load, the topology scheme of the LCC-S compensated IPT system is shown in Fig. 1. L_{P} and L_{S} are the self-inductances of the transmitting and receiving coils and M is the mutual inductance between the two coils. S_1-S_4 consist of full bridge inverter. L_{P1}, C_{P1} and C_{P2} are the primary side resonant elements, forming the LCC compensation network. C_{S1} is the secondary side compensation component, in series with receiving coil. Here, U_{d} is original DC input voltage source, while U_{AB} and I_{AB} are high frequency output voltage and current of inverter. R_{O} is the load resistance. D_1-D_4 are the secondary-side rectifier diodes and C_f is filter capacitor. In order to simplify the analysis, the parasitic resistances in the inductors and capacitors are omitted.

Owing to the filtering function of compensation network, the fundamental harmonic approximation (FHA) is employed. When the duty cycle of the inverter is 50%, the relationship between input voltage U_{AB} of resonant tank and the input DC voltage U_d can be expressed as follow

$$U_{AB} = \frac{2\sqrt{2}}{\pi} U_d \tag{1}$$

The ac load R_E, including the diode rectifier, filter capacitor, and resistive load, can be calculated as

$$R_E = \frac{8}{\pi^2} R_O \tag{2}$$

In the IPT system, the loosely coupled transformer (LCT) plays a key role in the output characteristics and efficiency. Two well-known models of the LCT called mutual inductance model (M-model) and T-model are widely used. In LCC-S compensation topology, to clarify the resonance relation in parameters design, T-model shown in Fig. 2 is employed. The apostrophe symbol "'" indicates the corresponding variables of the secondary side converted to primary side.

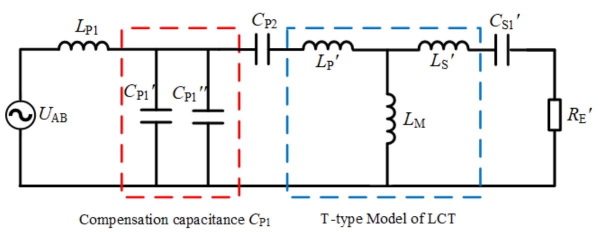

FIGURE 2. **T equivalent model of LCC-S compensation topology.**

A. LOAD-INDEPENDENT CURRENT OUTPUT CHARACTERISTICS

Base on T-mode of the LCT, L_P' and L_S' in Fig. 2 are the reflected leakage inductances of primary and secondary coils respectively while L_M stands for the primary reflected mutual inductance and k is the coupling coefficient. n denotes turns ratio of ideal transformer. In terms of circuit principles, the following equations can be obtained

$$\begin{cases} L_P' = (1-k)L_P \\ L_S' = (1-k)n^2 L_S \\ L_M = nM \\ n = \sqrt{L_P/L_S} \end{cases} \tag{3}$$

C_{S1}' and R_E' are the primary-referred value of C_{S1} and R_E, respectively and can be derived as

$$\begin{cases} C_{S1}' = C_{S1}/n^2 \\ R_E' = n^2 R_E \end{cases} \tag{4}$$

C_{P1} in Fig. 2 is split into two parts–C_{P1}' and C_{P1}''. In this paper, C_{P2}, C_{S1}' and C_{P1}'' are designed to resonate with the leakage inductance and mutual inductance of LCT respectively, i.e. C_{P2} series resonate with L_P', C_{S1}' series resonate with L_S', while C_{P1}'' and L_M make up a parallel resonant tank. The resonant frequencies equal to the system operating frequency f_S and its angular frequency is ω_S. Then the following equation can be obtained:

$$\omega_S = \frac{1}{\sqrt{L_M C_{P1}''}} = \frac{1}{\sqrt{L_P' C_{P2}}} = \frac{1}{\sqrt{L_S' C_{S1}'}} \tag{5}$$

According the characteristic of an LC resonant tank, i.e. constant voltage input convert to constant current output, C_{P1}' is selected to resonate with L_{P1} at ω_S as

$$C_{P1}' = \frac{1}{\omega_S^2 L_{P1}} \tag{6}$$

and the load-independent current output I_{LCP1}' after C_{P1}' can be yielded as

$$I_{LCP1}' = -j\frac{U_{AB}}{\omega_S L_{P1}} \tag{7}$$

Since compensated capacitance C_{P2} and the transmitting coil are connected in series, the current flowing through the transmitting coil can be calculated as follows:

$$\begin{aligned} I_{LP} = I_{CP2} &= I_{LCP1}'\left(\frac{R_E'}{j\omega_S L_M} + 1\right) \\ &= -j\frac{U_{AB}}{\omega L_{P1}} - \frac{nU_{AB}R_E}{k\omega_S^2 L_{P1} L_P} \end{aligned} \tag{8}$$

Equation 8 suggests that the current across transmitting coil increase with the load, different from conventional primary LCC compensate topology.

Theoretically, when all resonances satisfy in (5), the current I_{RE}' over R_E' is the same as I_{LCP1}'. In terms of the relationship between primary-referred value of R_E' and the actual load R_E, the realistic current I_{RE} can be yielded

$$I_{RE} = nI_{RE}' = -j\frac{nU_{AB}}{\omega_S L_{P1}} \tag{9}$$

The output current I_{RO} through R_O can be yielded

$$I_{RO} = \frac{8}{\pi^2}\frac{nU_d}{\omega_S L_{P1}} \tag{10}$$

Equation (10) implies I_{RO} has nothing to do with R_O. The LCC-S compensated IPT system possesses one more degree of freedom—L_{P1}, which gets rid of strict coil size limitations. Assuming switch components are ideal and ignoring components loss, the average power transferred to load can be given as

$$P_{RO} = \frac{64}{\pi^4}\frac{U_d^2 L_P}{\omega_S^2 L_{P1}^2 L_S} R_O \tag{11}$$

B. ZVS REALIZATION

In practical scenarios, in order to reduce the switching loss and improve system efficiency, zero voltage switching (ZVS) condition is prefer to achieve and the system input impedance should be inductive. Under perfect resonant condition the equivalent impedance seen from the input port of compensation network is

$$Z_{in} = \frac{U_{AB}}{I_{AB}} = j\omega L_{P1} + \left(\frac{1}{j\omega C_{P1}'} \parallel R_E'\right) \tag{12}$$

where the operator "//" represents the parallel calculation of impedance. Substituting (2) and (4) into (12), Z_{in} can be depicted as

$$Z_{in} = \frac{\pi^2\omega_S^2 L_{P1}^2 L_S^2}{64 L_P^2 R_O^2 + \pi^4 \omega_S^2 L_{P1}^2 L_S^2}(8n^2 R_E + j\pi^2\omega_S L_{P1}) \tag{13}$$

The input impedance angle θ can obtained as

$$\theta = \frac{180^\circ}{\pi} \arctan \frac{\pi^2 \omega_S L_{P1}}{8n^2 R_E} \tag{14}$$

It can be seen from (14) that the input impedance Z_{in} is always inductive and the inductance L_{P1} and the coil ratio n exert an influence on the input impedance angle θ. Fig. 3 shows the actual input phase angle with respect to varied load and different size combination of L_{P} and L_{S}. In accordance with (14), it is found that the input phase angle decreases quickly with the increase of load and a larger coil ratio n makes the input impedance angle smaller. This means that larger L_{P} or smaller L_{S} is a better choice for efficiency improvement, which are consistent with most applications. Considering the space constraints of the coils simultaneously, the self-inductance of transmitting coil is three times that of receiving coil, i.e. n is determined around 1.732 temporarily. It can be seen from Fig. 3 that when R_{E} is greater than 70 Ω, the impedance angle does not exceed 30°, while greater than 150 Ω, the variation of input impedance angle is inconspicuous.

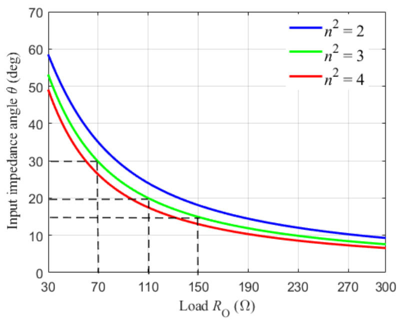

FIGURE 3. Input impedance angle θ varied with load R_{O} and turn ratio n.

For clarity, the compensation parameters tuning methods for L_{P1}, C_{P1}, C_{P2} and C_{S1} are rearranged by the equations below:

$$\begin{cases} L_{P1} = \dfrac{8}{\pi^2}\sqrt{\dfrac{L_P}{L_S}}\dfrac{U_{\text{d}}}{\omega_S I_{RO}} \\ C_{P1} = \dfrac{1}{\omega_S^2 L_{P1}} + \dfrac{1}{k\omega_S^2 L_P} \\ C_{P2} = \dfrac{1}{\omega_S^2 (1-k) L_P} \\ C_{S1} = \dfrac{1}{\omega_S^2 (1-k) L_S} \end{cases} \tag{15}$$

Compared with conventional LCC-S compensation topologies, the entire resonant tank composed of proposed LCC-S compensation network are more obvious to show a CCO characteristic. Based on (14), the output current can be altered by employing different L_{P1} and C_{P1}, which is not constrained by the LCT parameters. Moreover, ZVS can be implemented naturally. This is very helpful to improve the efficiency of the IPT system. Both cost and size of system can be reduced.

III. TOPOLOGY DESIGN ENHANCE OF MISALIGNMENT TOLERANCE

The output current of the novel proposed LCC-S system has nothing to coupling coefficient under perfect compensation to leak mutual inductances. However, it is universal that transmitting and receiving coils are hardly well aligned. Misalignment is inevitable in most cases, which changes the mutual inductances dramatically and leads to instability and reduction in efficiency. Therefore, the development of misalignment tolerance is important and significant.

The currents across L_{P1}, L_{P} and L_{S} with respect to the coupling coefficient are shown in the Fig. 4. Two information are exposed: The tolerance performance of misalignment is unsatisfactory and large currents are ineluctable. The current across inductances and the voltage over capacitors are both accrescent dramatically. The system may be destroyed by the current surges in coils and inverter. When the coupling coefficient drops to zero, the system is similar to SS topology. For a consummate IPT system, it is necessary to tolerate not only a large variation of load, but also a wide range of coupling coefficient.

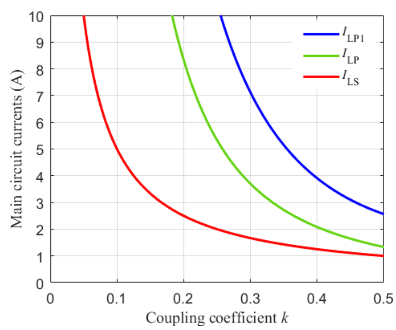

FIGURE 4. Currents of main branches against varied coupling coefficient k.

A. MODIFIED PARAMETER TUNING METHOD

According to the fully tuning method in the Section II, k_0 is selected to represent the coupling coefficient under normal operation. The output current no longer conforms to (10) due to the misalignment. In this scenarios, T-model is renovated and elaborated firstly, as shown in Fig. 5. Some previous works have pointed out that design methods with detuned compensated parameters are simple but efficacious to reduce the power fluctuation [4], [24]. Owing to compensating the coupling transformer, C_{P1}'', C_{P2} and C_{S1} are initially designed with k_0 when well aligned. Resonant L_{P1} and C_{P1}' determine the output current, which are suitable for misalignment optimization study. Taking the impedance of L_{P} as a reference, the detuned impedance factors of L_{P1} and C_{P1} are defined as follows:

$$\alpha = \frac{|Z_{LP1\_de}|}{|Z_{LP}|} \tag{16}$$

$$\beta = \frac{|Z_{LP}|}{|Z_{CP1\_de}|} \tag{17}$$

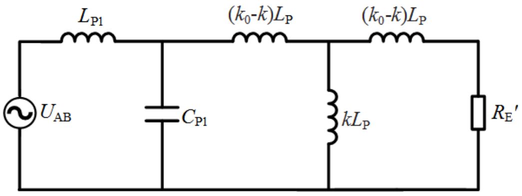

FIGURE 5. T equivalent model when misalignment.

The quality factor of the series-compensated receiver circuit is defined as

$$Q = \frac{\omega_0 L_P}{R_E'} \tag{18}$$

Thus, the reflected impedance Z_{r_mis} to $L_{P1}C_{P1}$ resonant tank can be described as

$$Z_{r\_mis} = \frac{k_0\,|Z_{LP}| + Q(k_0^2 - k^2)Z_{LP}}{k_0 Q - j} \tag{19}$$

The total input impedance Z_{in} can be given as

$$Z_{in} = Z_{LP1} + \frac{Z_{PC1} Z_{r\_mis}}{Z_{PC1} + Z_{r\_mis}} \tag{20}$$

Replacing the L_{P1} and C_{P1} with α and β, Z_{in} can be expressed as (21), shown at the bottom of the page.

Based on Kirchhoff's current law, the current in the transmitting coil can be updated as (22), shown at the bottom of the page.

Similarly, the current on the receiver side can be described as follows:

$$I_{RE} = I_S = nI_S' = \frac{nU_{AB}}{\left[\frac{Ak_0}{k} - \frac{A-\alpha}{k_0}k\right] Z_{LP} + \frac{A}{Qk}\,|Z_{LP}|} \tag{23}$$

where $A = \alpha + (1\text{-}\alpha\beta)\,k_0$.

In (23), the current of load is relevant to variables of α, β and coupling coefficient. The introduction of α, β makes the transfer impedance Z_{trans} of terminal load and DC voltage source controllable and convenient. The rms amplitude of output current is discussed as

$$I_{Amp}(\alpha, \beta, k) = |I_{RE}| = \frac{|U_{AB}|}{|Z_{trans}|} \tag{24}$$

By calculating the minimum value of the transfer impedance Z_{trans}, The k for maximum I_{Amp} can be obtained. The derivative of Z_{trans} with respect to k can be calculated as

$$\frac{\partial Z_{Amp}}{\partial k} = -2A^2 \frac{(k_0^2 + Q^{-2})}{k^3} + 2(A-\alpha)^2 \frac{k}{k_0^2} \tag{25}$$

Solving $\partial Z_{Amp}/\partial k = 0$, the extreme point can be obtained as

$$k_{opt} = \sqrt[4]{k_0^2 + Q^{-2}} \sqrt{\left| k_0 + \frac{\beta}{1-\alpha\beta} \right|} \tag{26}$$

k_{opt} is the coupling coefficient at maximum output current. The relationship between k_{opt} and detuning parameters α, β is shown in Fig. 6 (a). From Fig. 6 (a), It can be observed that the k_{opt} becomes zero when L_{P1} and C_{P1}' are in resonance. When the detuning factors deviates further from resonance state, the k_{opt} becomes increases. Both relatively small α, β should not be employed concurrently, because k_{opt} is limited to 1. Assuming the demand output fluctuation is within 10% and the effective range of k is (k_{min}, k_{max}), which includes the extreme coupling point k_{opt}. Three corresponding output currents $I_{RO}(k_{min})$, I_{RO} (k_{opt}) and I_{RO} (k_{max}) are obtained respectively.

To ensure a smooth output current profile around nominal coupling and load condition, the parameters α, β must jointly help meet the restrictions depicted by (27), where I_{nom} is the nominal current. Generally, coupling coefficient will reduce when misalignment, thus, k_{max} is picked to equal to the nominal coupling coefficient k_0.

$$\begin{cases} I_{RO}(k_{max}) = I_{nom} \\ I_{RO}(k_{opt}) = 1.1 I_{nom} \\ I_{RO}(k_{min}) = 0.9 I_{nom} \end{cases} \tag{27}$$

The expression of I_{RO} is so complicated that numerical simulation tools, such as MATLAB is utilized to analyze the influence of detuned compensated resonance. The main parameters utilized in the simulations are given by Tab. 1 and 2. With nominal current of 1 A, $I_{RO}(k_{opt})$ and I_{RO} (k_{max}) against various detuning α, β are shown in Fig. 6 (b) and Fig. 6 (c). In terms of Fig. 6 (b), it can be seen that the maximum current of $I_{RO}(k_{opt})$ tends to infinity when L_{P1} and C_{P1} resonates. The slope rate on either side of resonate conditions decrease dramatically. Fig. 6 (c) suggests that the output current decreases smoothly deviate from the resonance but around 1A. Therefore, feasible α, β solutions λ_1(0.186, 8.344) and λ_2(0.229, 5.992) are numerically solved as shown in Fig. 7, satisfying equations in (27) simultaneously. The two solutions are distributed on different sides of L_{P1} and C_{P1} resonance curve.

The curves of output current and input phase angle of λ_1 and λ_2 are shown in Fig. 8. The tolerance characteristics of misalignment can be reflected by k_{min}. The k_{min} of λ_2 is 0.188, descending 62.4% of coupling coefficient in normal

$$Z_{in} = \frac{\left[\alpha k_0(1+\beta) + Q(k_0^2 - k^2)\right] Z_{LP} + \left[\alpha + k_0 - \alpha\beta Q(k_0^2 - k^2)\right] |Z_{LP}|}{k_0(1+\beta) + \left[\beta Q(k_0^2 - k^2) - 1\right] j} \tag{21}$$

$$I_P = \frac{(k_0 Q - j)U_{AB}}{Q\left[\alpha k_0 + (1-\alpha\beta)(k_0^2 - k^2)\right] Z_{LP} + \left[\alpha + k_0(1-\alpha\beta)\right] |Z_{LP}|} \tag{22}$$

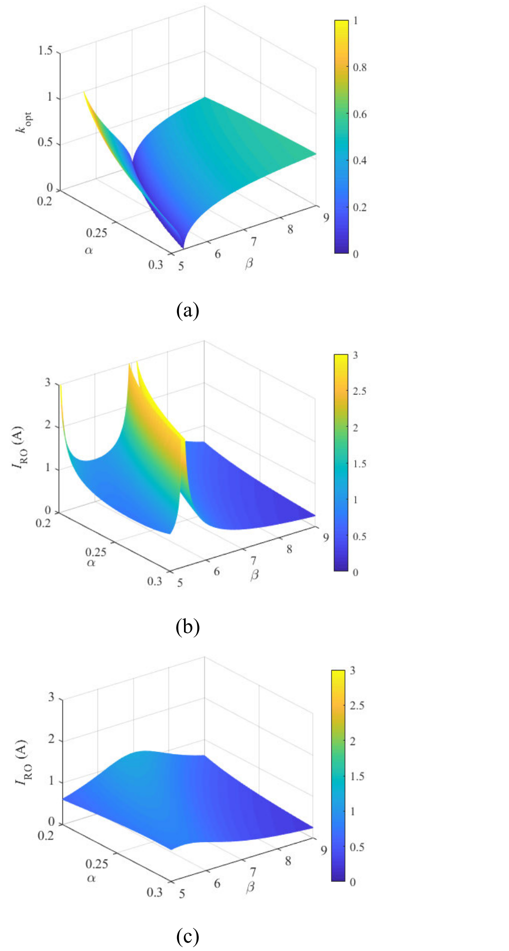

FIGURE 6. k_{opt}(a), I_{RO} when $k = k_{opt}$ (b) and I_{RO} when $k = k_{MAX}$ (c) versus α, β.

TABLE 1. Some critical parameters adopted in the simulation.

Symbol	Parameters	Value
U_d	input voltage	44.42 V
L_P	primary self-inductance of the LCT	540 uH
L_S	secondary self-inductance of the LCT	180 uH
R_O	rated resistive load	100 Ω
P_{RO}	output power	100 W

TABLE 2. Circuit components for different optimized LCC-S compensation topologies.

Symbol	L_{P1}/uH	C_{P1}/nF	C_{P2}/nF	C_{S1}/nF
CVO Type	76.96	45.56	7.57	19.48
CCO Type	116.79	43.00	12.99	38.96
Modified Type	100.44	54.17	12.99	38.96

operation and indicating an effective improvement of misalignment tolerance. However, investigating the input phase angle of the inverter, its phase angle is always capacitive and varies in a large range. From Fig. 8, we can see that the input impedance of λ_2 is inductive and ZVS can be achieved within the range of misalignment. It can be seen that the change

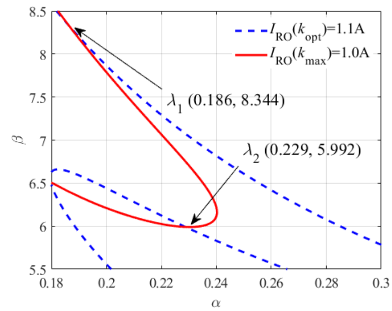

FIGURE 7. Numerical solutions of α, β to meet fluctuation demand.

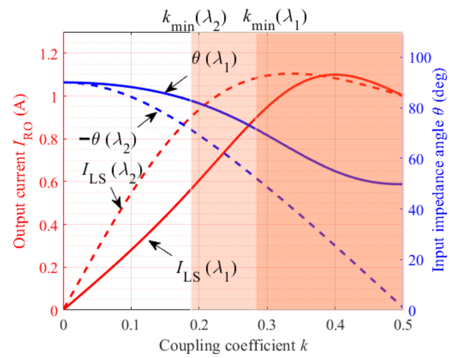

FIGURE 8. Input impedance angle θ and output current I_{RO} varied with k.

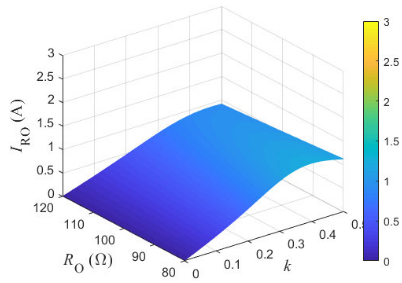

FIGURE 9. Misalignment tolerance versus both load R_O and coupling coefficient k.

of input phase angle from k_{min} to k_{max} is small. For sets of optimized λ_1, a wide flat region is obtained, where k_{min} of λ_1 is 0.284 and k_{opt} is 0.402. The values of λ_1(0.186, 8.344) indicate that a small resonance inductance L_{P1} and a large resonance capacitance C_{P1} are what we want. With properly design, the fluctuation of current is only 10% when the coupling coefficient varies almost 176.06% (from 0.284 to 0.5).

Since the parameters design is based on nominal load condition, if R_O deviates from its nominal value, the CCO misalignment characteristics will be affected. However, as shown in Fig. 9, by implementing the optimal parameters, the fluctuation of current is still small and can be neglected. When Ro changes by 20%, the current fluctuates by 8.5% at $k = 0.5$, $Ro = 120$ Ω, and 22.2% at $k = 0.4$, $Ro = 80$ Ω, indicating a good CCO misalignment characteristics against varied load and coupling coefficient simultaneously. The robustness to coupling coefficient can be guaranteed and it can still be

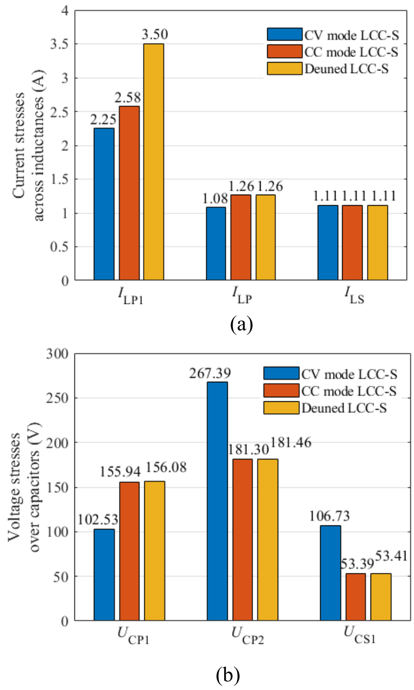

FIGURE 10. Stresses on inductors (a) and capacitors, (b) under three optimized LCC-S compensation topologies.

regarded as a CCO system. This makes the design of back-end converter easier and the complicated and troublesome control circuit can be omitted.

B. STRESSES ACROSS RESONANT COMPONENTS

The current stresses across inductances and the voltage stresses over capacitors both have a great impact on system efficiency and cost. To fairly compare the component stresses between LCC-S IPT systems with different parameters optimization, the input voltage, operation frequency, LCT and resistive load should be identical as listed in Tab. 1. The traditional LCC-S topology with the characteristic of constant voltage output (CVO) is the most widely employed and can be used as a comparison. All IPT systems are optimized to the same output power. The parameters tuning method of LCC-S compensation topology with CVO can refer to [11]. According to the discussion before, the parameters of proposed LCC-S topology with CCO characteristic and modified design to enhance misalignment tolerance are applied. Three sets of compensation parameters are tabulated in Tab. 2. On the basis of circuit theories, the stresses on inductors and capacitors can be obtained as shown in Fig. 10.

For CVO type LCC-S compensated system, the current stresses on L_{P1} and L_P are relatively small, but the voltage stress on C_{P2} is far exceed other capacitors stresses. Processing same transfer power, the current stresses of CCO type LCC-S compensation topologies are approximate, similar small current stresses across inductances. However, the voltage stresses over C_{P2} and C_{S1} is 181.3 V and 53.39 V, only 67.8% and 50% of CVO type. Although the voltage of C_{P1} increases, the stresses of every compensation components are more balanced and the total stresses on the capacitors of CCO type are smaller than that of CVO type. When L_{P1} is not resonant with C_{P1}, the current through L_{P1} is 3.5 A, which increases about 35.66%. For the modified topology, the stresses mainly increase due to the introduction of some reactive power. The primary side loss will increase with the misalignment. On the whole, the total stresses on the components of modified LCC-S are reasonable and appropriate.

IV. EXPERIMENTAL VERIFICATION

To further verify the theoretical analysis, a 100 W LCC-S compensated IPT prototype is built and shown in Fig. 11. The employed parameters are tabulated in Tab. 1 and Tab. 2. A slightly larger $U_d = 47.07$ V was determined to make the output current 1 A when R_O and k_0 are 100 Ω and 0.5, respectively. Power MOSFET IPW90R120C3 is selected as the power switch, and TMS320F28335 DSP is implemented as controller to generate the square-wave voltage. The LCT is composed of two circular pad coils. L_{P1}, C_{P1}, C_{P2} and C_{S1} are tuned at k_0. On the basis of (16) and (17), L_{P1}' and C_{P1}' were detuned by α and β.

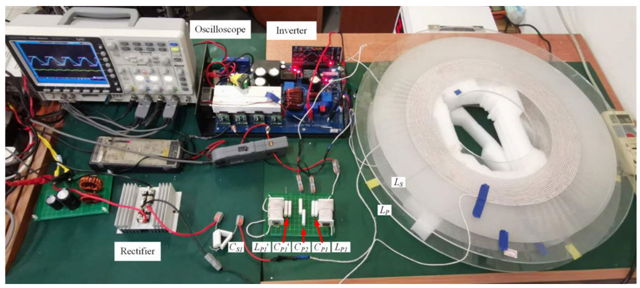

FIGURE 11. Prototype of the proposed LCC-S compensated system.

With the tuned L_{P1} and C_{P1}, the output voltage and current waveforms of the inverter are shown in Fig. 12. The fundamental component of voltage leads that of current, indicating an equivalent inductive load for the inverter. The load resistance is 50 Ω, 80 Ω, 100 Ω, and the corresponding input phase angle is 25.70° (0.84 μs), 17.75° (0.58 μs), 15.91° (0.52 μs). It is obvious that the ZVS of MOSFETs has be realized and such a leading angle is quite desired with extremely small reactive power. Fig. 12 also shows the output current waveforms of load resistance when the load is different. The I_{RO} is 1.032A, 1.012A and 1.00A respectively. The load decreases by 50%, but the output current only increases by 3.2%, illustrating an excellent CCO characteristic of LCC-S compensated topology. The transient states of voltage and current in two different load stages are shown in Fig. 13. After an instant surge, i_{RO} returns to constant current. Fig. 14 exhibits the profile of output current i_{RO} with respect to the load. When R_O reduces from 100 Ω to 20 Ω, I_{RO} increases linearly from 1 to 1.05 A. The efficiency of the system is above 86%, holding a high level in the wide range of load.

Considering conditions of misalignment, the detuned L_{P1} and C_{P1} are adopted, where L_{P1} is 100.44 μH and C_{P1}

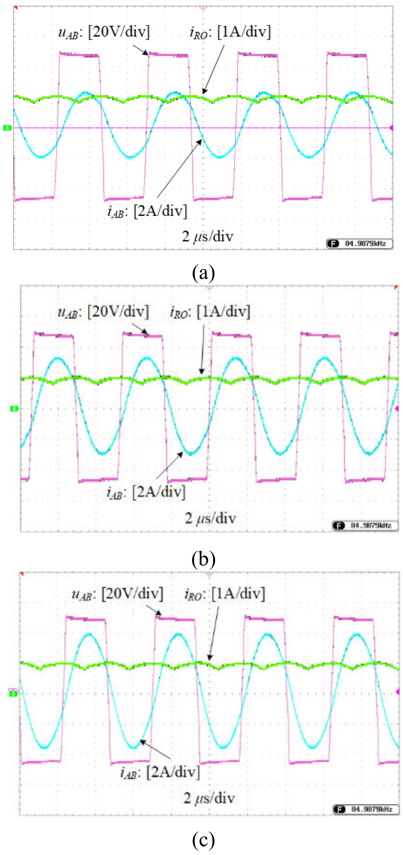

FIGURE 12. Waveforms of system under various load (a) $R_O = 50\ \Omega$, (b) $R_O = 80\ \Omega$, (c) $R_O = 100\ \Omega$.

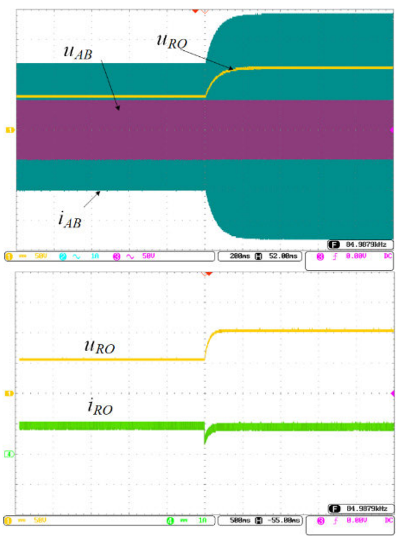

FIGURE 13. CCO characteristic of proposed LCC-S compensation topology.

is 54.17 nF. The component stresses under two sets of parameters are compared with the same transmission power, as shown in Fig. 15 and 16. When the receiving coil is mostly aligned with the transmitting coil ($k = 0.5$), the voltage over C_{P2} and C_{P1} of detuned system are almost similar to the tuned system. The voltage amplitude on C_{P1} reaches 220 V, while that on C_{S1} is only about 80 V. The approximate current

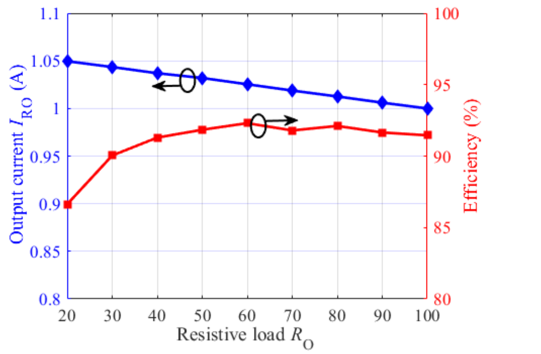

FIGURE 14. Output current and transmission efficiency versus load R_O with tuned parameters.

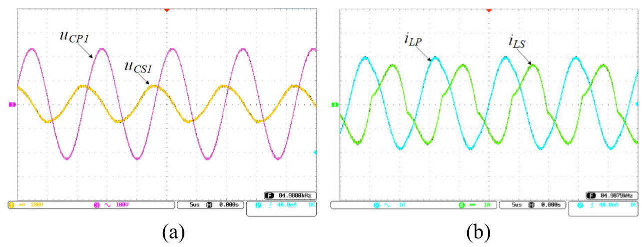

FIGURE 15. (a) Voltages over C_{P1}, C_{S1} and (b) currents through L_P, L_S with tuned LCC-S compensation topology.

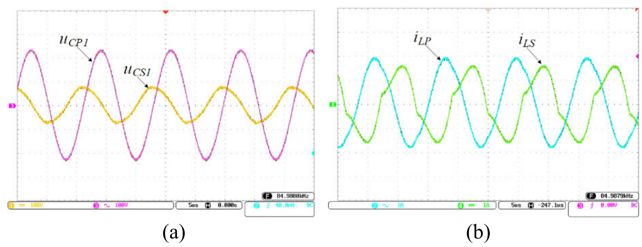

FIGURE 16. (a) Voltages over C_{P1}, C_{S1} and (b) currents through L_P, L_S with detuned LCC-S compensation topology.

stresses happen to the two coils. The amplitude of the current flowing through the transmitting coil reaches 2 A, while that of the receiving coil is about 1.6 A. Although due to the introduction of reactive power, all stresses are small and acceptable.

The experimental results of misalignment tolerance capability are exhibited in Fig. 17. Compared with the resonant L_{P1} and C_{P1}, the parameters under detuning cause larger input impedance phase angle. Under the same rated conditions, i.e. $R_O = 100\ \Omega$ and $k = 0.5$, the input impedance angle is 42.48° (1.40 μs) and the output current of the inverter reaches 2A, which is twice of that under resonance condition. When the misalignment increases to $k = 0.394$ and $k = 0.293$, the lagging phase angle becomes larger, close to 46.51° (1.52 μs) and 58.75° (1.92 μs) respectively. Within the entire misalignment range from 0.5 to 0.3, the inverter bridge always operates at the soft-switching state. The profile of load current I_{RO} with respect to coupling coefficient is shown in Fig. 18. In detuned LCC-S system, the output current rises slightly and then decreases along with the deviation of coils. The maximum output current is 1.075 A around $k_{opt} = 0.4$. When

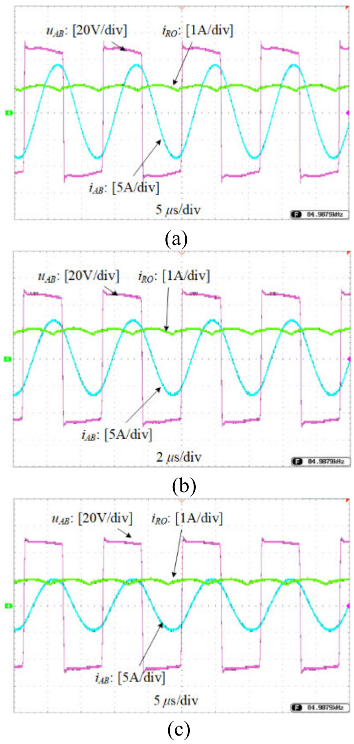

FIGURE 17. Waveforms of system when (a) $k = 0.293$, (b) $k = 0.394$, (c) $k = 0.496$.

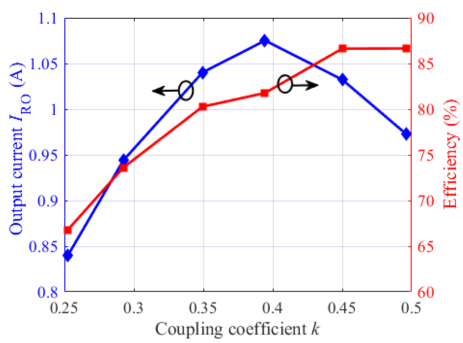

FIGURE 18. Output current and transmission efficiency versus coupling coefficient k with detuned parameters.

k drops to 0.293, the output current fluctuation is 5.6%. The constant output current is maintained with only a small peak-to-peak fluctuation of 0.13 A. The experimental results agree well with theoretical analysis, demonstrating the rightness of previous analysis. The efficiency of the detuned system is also measured as shown in Fig. 18. It can be observed that the efficiency of detuned LCC-S system decays with the decrease of coupling coefficient. Because the introduction of more reactive power, the currents of each branch increase and the power loss of following parts will raise: the switching loss of inverter, compensation network, transmitting coil and receiving coil. Another reason is the application of high-voltage devices featured high forward voltage or turn-on resistance, including 900 V MOSFETs (IPW90R120C3) and 600 V diodes (DSEI 2×101). When used for low power verification, it will cause higher losses compared to a design with lower voltage devices. For optimized detuned system, high efficiency over 73% is maintained in the range of k from 0.293 to 0.5.

V. CONCLUSION

In this study, an optimized LCC-S compensation topology for IPT system is proposed. Free from the constraints imposed by the LCT, it provides excellent load-independent current output characteristic. When load drops by 50%, the output current only increases by 5%. The inherent ZVS characteristics of LCC-S system drastically reduced high frequency switching loss and simplified thermal circuit. Compared with double-sided LCC compensation topology, less compensation components are needed in LCC-S topology, which improve system power density and efficiency. Based on the analysis of detuned conditions on L_{P1} and C_{P1}, a stable transmission power system against misalignment was identified. Experimental results verify that the current fluctuation is no more than 7.5% within almost 170% of coupling coefficient variation (from 0.293 to 0.5). Another advantage is that the currents of each branch are limited, which protects the IPT system. The experimental results show good agreement with theoretical analysis.

REFERENCES

[1] D. Patil, M. K. McDonough, J. M. Miller, B. Fahimi, and P. T. Balsara, "Wireless power transfer for vehicular applications: Overview and challenges," *IEEE Trans. Transport. Electrific.*, vol. 4, no. 1, pp. 3–37, Mar. 2018.

[2] R. Wu, W. Li, H. Luo, J. K. O. Sin, and C. Patrick Yue, "Design and characterization of wireless power links for Brain–Machine interface applications," *IEEE Trans. Power Electron.*, vol. 29, no. 10, pp. 5462–5471, Oct. 2014.

[3] R. Tavakoli and Z. Pantic, "Analysis, design, and demonstration of a 25-kW dynamic wireless charging system for roadway electric vehicles," *IEEE J. Emerg. Sel. Topics Power Electron.*, vol. 6, no. 3, pp. 1378–1393, Sep. 2018.

[4] J. Zhao, T. Cai, S. Duan, H. Feng, C. Chen, and X. Zhang, "A general design method of primary compensation network for dynamic WPT system maintaining stable transmission power," *IEEE Trans. Power Electron.*, vol. 31, no. 12, pp. 8343–8358, Dec. 2016.

[5] G. de Freitas Lima and R. B. Godoy, "Modeling and prototype of a dynamic wireless charging system using LSPS compensation topology," in *Proc. Brazilian Power Electron. Conf. (COBEP)*, Nov. 2017, pp. 1–6.

[6] Y. Yao, X. Liu, Y. Wang, and D. Xu, "LC/CL compensation topology and efficiency-based optimisation method for wireless power transfer," *IET Power Electron.*, vol. 11, no. 6, pp. 1029–1037, May 2018.

[7] X. Qu, Y. Jing, H. Han, S.-C. Wong, and C. K. Tse, "Higher order compensation for Inductive-Power-Transfer converters with constant-voltage or constant-current output combating transformer parameter constraints," *IEEE Trans. Power Electron.*, vol. 32, no. 1, pp. 394–405, Jan. 2017.

[8] L. Zhao, S. Ruddell, D. J. Thrimawithana, U. K. Madawala, and P. A. Hu, "A hybrid wireless charging system with DDQ pads for dynamic charging of EVs," in *Proc. IEEE PELS Workshop Emerg. Technol., Wireless Power Transf. (WoW)*, May 2017, pp. 1–6.

[9] S. Bandyopadhyay, P. Venugopal, J. Dong, and P. Bauer, "Comparison of magnetic couplers for IPT-based EV charging using multi-objective optimization," *IEEE Trans. Veh. Technol.*, vol. 68, no. 6, pp. 5416–5429, Jun. 2019.

[10] F. Lu, H. Zhang, H. Hofmann, W. Su, and C. C. Mi, "A dual-coupled LCC-compensated IPT system with a compact magnetic coupler," *IEEE Trans. Power Electron.*, vol. 33, no. 7, pp. 6391–6402, Jul. 2018.

[11] M. Kim, D.-M. Joo, and B. K. Lee, "Design and control of inductive power transfer system for electric vehicles considering wide variation of output voltage and coupling coefficient," *IEEE Trans. Power Electron.*, vol. 34, no. 2, pp. 1197–1208, Feb. 2019.

[12] Y. Wang, Y. Yao, X. Liu, D. Xu, and L. Cai, "An LC/S compensation topology and coil design technique for wireless power transfer," *IEEE Trans. Power Electron.*, vol. 33, no. 3, pp. 2007–2025, Mar. 2018.
[13] X. Qu, H. Chu, Z. Huang, S.-C. Wong, C. K. Tse, C. C. Mi, and X. Chen, "Wide design range of constant output current using double-sided LC compensation circuits for inductive-power-transfer applications," *IEEE Trans. Power Electron.*, vol. 34, no. 3, pp. 2364–2374, Mar. 2019.
[14] W. Zhang and C. C. Mi, "Compensation topologies of high-power wireless power transfer systems," *IEEE Trans. Veh. Technol.*, vol. 65, no. 6, pp. 4768–4778, Jun. 2016.
[15] W. Li, H. Zhao, J. Deng, S. Li, and C. C. Mi, "Comparison study on SS and double-sided LCC compensation topologies for EV/PHEV wireless chargers," *IEEE Trans. Veh. Technol.*, vol. 65, no. 6, pp. 4429–4439, Jun. 2016.
[16] M. Kissin, C.-Y. Huang, G. A. Covic, and J. T. Boys, "Detection of the tuned point of a fixed-frequency LCL resonant power supply," *IEEE Trans. Power Electron.*, vol. 24, no. 4, pp. 1140–1143, Apr. 2009.
[17] J. Hou, Q. Chen, X. Ren, X. Ruan, S.-C. Wong, and C. K. Tse, "Precise characteristics analysis of series/series-parallel compensated contactless resonant converter," *IEEE J. Emerg. Sel. Topics Power Electron.*, vol. 3, no. 1, pp. 101–110, Mar. 2015.
[18] Q. Zhu, L. Wang, Y. Guo, C. Liao, and F. Li, "Applying LCC compensation network to dynamic wireless EV charging system," *IEEE Trans. Ind. Electron.*, vol. 63, no. 10, pp. 6557–6567, Oct. 2016.
[19] Z. Pantic, S. Bai, and S. M. Lukic, "ZCS *LCC*-compensated resonant inverter for inductive-power-transfer application," *IEEE Trans. Ind. Electron.*, vol. 58, no. 8, pp. 3500–3510, Aug. 2011.
[20] T. Kan, F. Lu, T.-D. Nguyen, P. P. Mercier, and C. C. Mi, "Integrated coil design for EV wireless charging systems using LCC compensation topology," *IEEE Trans. Power Electron.*, vol. 33, no. 11, pp. 9231–9241, Nov. 2018.
[21] A. Ramezani, S. Farhangi, H. Iman-Eini, B. Farhangi, R. Rahimi, and G. R. Moradi, "Optimized LCC-series compensated resonant network for stationary wireless EV chargers," *IEEE Trans. Ind. Electron.*, vol. 66, no. 4, pp. 2756–2765, Apr. 2019.
[22] J. Lu, G. Zhu, D. Lin, S.-C. Wong, and J. Jiang, "Load-independent voltage and current transfer characteristics of high-order resonant network in IPT system," *IEEE J. Emerg. Sel. Topics Power Electron.*, vol. 7, no. 1, pp. 422–436, Mar. 2019.
[23] S. Li, W. Li, J. Deng, T. D. Nguyen, and C. C. Mi, "A double-sided LCC compensation network and its tuning method for wireless power transfer," *IEEE Trans. Veh. Technol.*, vol. 64, no. 6, pp. 2261–2273, Jun. 2015.
[24] H. Feng, T. Cai, S. Duan, J. Zhao, X. Zhang, and C. Chen, "An LCC-compensated resonant converter optimized for robust reaction to large coupling variation in dynamic wireless power transfer," *IEEE Trans. Ind. Electron.*, vol. 63, no. 10, pp. 6591–6601, Oct. 2016.
[25] Y. Yao, Y. Wang, X. Liu, K. Lu, and D. Xu, "Analysis and design of an S/SP compensated IPT system to minimize output voltage fluctuation versus coupling coefficient and load variation," *IEEE Trans. Veh. Technol.*, vol. 67, no. 10, pp. 9262–9272, Oct. 2018.
[26] R. Mai, Z. Yan, Y. Chen, S. Liu, and Z. He, "A hybrid transmitter-based efficiency improvement controller with full-bridge dual resonant tank for misalignment condition," *IEEE Trans. Power Electron.*, vol. 35, no. 1, pp. 1124–1135, Jan. 2020.
[27] C. Xia, W. Wang, S. Ren, X. Wu, and Y. Sun, "Robust control for inductively coupled power transfer systems with coil misalignment," *IEEE Trans. Power Electron.*, vol. 33, no. 9, pp. 8110–8122, Sep. 2018.
[28] H. Feng, T. Cai, S. Duan, X. Zhang, H. Hu, and J. Niu, "A dual-side-detuned series–series compensated resonant converter for wide charging region in a wireless power transfer system," *IEEE Trans. Ind. Electron.*, vol. 65, no. 3, pp. 2177–2188, Mar. 2018.

JUNFENG YANG (Member, IEEE) received the B.S. degree in electrical engineering from Beijing Jiaotong University, Beijing, China, in 2012, where he is currently pursuing the Ph.D. degree in electrical engineering. His research interests include power electronics and wireless power transfer.

XIAODONG ZHANG received the M.Sc. degree in communication and information systems from Tianjin University, Tianjin, China, in 1991, and the Ph.D. degree in electromagnetic compatibility from Beijing Jiaotong University, Beijing, China, in 2012. Since 1993, he has been with the School of Electrical Engineering, Beijing Jiaotong University. His research interests include electromagnetic compatibility, power electronics, and wireless power transfer.

KAIJIAN ZHANG was born in Beijing, China, in 1996. He received the B.S. degree in mechanical and electronics engineering from Beijing Jiaotong University, Beijing, in 2018. He is currently pursuing the M.S. degree with the School of Computer Science and Engineering, University of New South Wales, Australia. His research interests include power electronics, the design and optimization of data structures, and database systems.

XIAOYAN CUI was born in 1958. She has been a Professor with the School of Automation, Beijing University of Posts and Telecommunications. Her research interests include wireless sensor networks and energy management.

CHAOQUN JIAO received the M.Sc. and Ph.D. degrees in electrical theory and new technology from North China Electric Power University, Hebei, China, in 2003 and 2006, respectively. Since 2006, he has been with the School of Electrical Engineering, Beijing Jiaotong University. His research interests include electrical theory and new technology, ultra high-voltage technology, and wireless power transfer.

XU YANG (Student Member, IEEE) received the B.Sc. degree from the School of Electrical and Electronics Engineering, Changchun University of Technology, Jilin, China, in 2010, and the M.Sc. degree in electrical engineering from Henan Polytechnic University, Henan, China, in 2013. He is currently pursuing the Ph.D. degree with the School of Electrical Engineering, Beijing Jiaotong University, Beijing, China. His research interests include wireless power transfer applications and power electronic converters.